Electron demagnetization and collisionless magnetic reconnection in $\beta_e \ll 1$ plasmas

J. D. Scudder[1] and F. S. Mozer[2]
[1] Dept. of Physics and Astronomy, University of Iowa
[2] Space Science Laboratory, UC Berkeley
Revised 7/25/2005
Accepted 8/8/2005
Physics of Plasmas

Abrupt, intense Electric Field Enhancements (EFEs) with $E > 100$mV/m surveyed over 3 years of Polar data are used to illustrate the occurrence and locales of non-guiding center demagnetization of thermal electrons in strongly inhomogeneous electric fields. A lower bound $E^*(a)$ on the perpendicular electric strength sufficient to cause non-gyrotropic effects on the electron pressure tensor is determined for EFE thickness $\Delta x = a\rho_e$. Minimum $E^*(a)$ occurs when $a \approx 1$. Of 258 observed EFEs, 15.3% (39) are demagnetizing (DEFEs) with $E \geq E^*(1)$. DEFEs occur within $3\times10^{-5} \leq \beta_e \leq 3\times10^{-2}$, while EFEs are found as low as $\beta_e = 10^{-8}$. While $E^*(1)$ does not depend on the ambient density, the DEFEs are organized by the density dependent inequality $\lambda_{De}/\rho_e < 1$ and are consistently understood as sites where the electron pressure tensor could become agyrotropic, enabling collisionless magnetic reconnection. The geophysical locales of the demagnetizing EFEs are not random, always occurring within magnetic cusp invariant latitudes, strongly concentrated at noon MLT and at orbit apogee near the nominal magnetopause.

RUNNING HEADER: Enabling Collisionless Magnetic Reconnection when $\beta_e \ll 1$

I. INTRODUCTION

Magnetic reconnection for collisionless plasmas is currently thought to be possible at sites where the electrons in the plasma can no longer be described with precision as a guiding center ordered fluid. At these sites the perpendicular electron flow velocity ceases to be a "field line velocity", precluding a detailed mapping in time of individual lines of force [1] and the cylindrical symmetry of the pressure tensor about the local magnetic field direction is broken. Examples with $\beta_e \geq 600$ at the separator at the Earth's magnetopause have been reported [2] where the thermal electron gyroradius $\rho_e = m_e w_e c/(eB)$ is much longer than the current layer scales and departures from electron gyrotropy have been detected [2]. The thermal gyroradius ($\rho_e \equiv \sqrt{\beta_e} d_e$) in such a $\beta_e \gg 1$ plasma will be much larger than the scale of the magnetic gradients since current channels tend to stop thinning at the electron inertial scale, $d_e = c/\omega_{pe}$. If electron demagnetization were only possible when $\beta_e \gg 1$, collisionless magnetic reconnection in low β_e plasmas like solar flares and machine plasmas would require time dependent agents beyond the narrowing of current channel, such as turbulence to affect the demagnetization of the electron fluid.

However, sharp spatial variations in **E** rather than in **B** can be the cause for disruption of the cylindrical symmetry of the electron pressure tensor. The best present indicators from observations [2], theory [3] and simulations [4,5] suggest that three unequal eigenvalues of the electron pressure tensor are required (not sufficient) to enable the topological evolution of collisionless magnetic reconnection. A corollary to this understanding is that topology preserving evolution of "frozen flux" should be expected unless the electron pressure tensor, an average of all the single particle motions [6], can become non-gyrotropic, and support a time averaged curl with components along **B**. In this paper we consider the possibility that disruption of the cylindrical symmetry of the electron pressure tensor is implied by at least some of the Electric Field Enhancements (EFEs) sampled by NASA's Polar spacecraft in Earth's magnetosphere. If such layers can be objectively identified they will be referred to as DEFEs for "demagnetizing" EFEs.

As electron fluids are generally subsonic in astrophysics, the assumption of guiding center ordering presumes that the variation of the *electromagnetic* field is smooth, with shallow gradients in **E** and **B**, across the gyroradius of the thermal electron of speed w_e and those nearby speeds that control the integrals of the pressure tensor elements. The pressure tensor is the repository in the moment description of the integrated effects of single particle dynamics of all types, whether guiding center ordered or not [6]. The symmetry of this tensor reflects a velocity space average of the single particle dynamics. Cylindrical symmetry of $\overleftrightarrow{\mathbf{P}}_j$ about a third axis aligned with **B** is often used as the assay of inferred guiding center particle dynamics for the j'th species of the plasma. Conversely three distinct eigenvalues for $\overleftrightarrow{\mathbf{P}}_j$ suggests the particle dynamics are non-gyrotropic and have been "demagnetized". Such pressure tensors can have a non-zero component along $\hat{\mathbf{b}}$ of the curl of their divergence and will contribute to the "collisionless" time rate of change of magnetic flux [1]. In a Maxwellian distribution the maximum of the integrands for pressure tensor elements occurs at a particle speed $v^* = \sqrt{2} w_e$; noticeable non-gyrotropic effects in the electron pressure moment

would appear to require the demagnetization of electrons with gyroradii in the vicinity of $\rho_e^* \simeq \sqrt{2} m_e w_e c/(eB)$. We make this estimate more quantitative below.

A. Electric Field Enhancements: EFE

Examples at Earth's magnetopause of intense, short duration Electric Fields Enhancement (EFE) perpendicular to the magnetic field have recently been published [7]. An announcement study of a preliminary sample of these strong electric field regions concluded they had scales either of electron skin depth, d_e or the much shorter electron Debye length, λ_{De}, if indeed they were even time stationary in their own frame of reference. The thicker presumption required atypically large relative motions past the spacecraft to explain their duration; assuming $O(\lambda_{De})$ scales was more consistent with the range of previously catalogued motions of the magnetopause. Recently it has been possible to "measure" [8] the spatial scale of one of these EFE structures (assuming it was time stationary in its own rest frame), showing that its half width was essentially the local thermal gyroradius, ρ_e that for ambient parameters was a few electron Debye lengths: $L \approx \rho_e = 7\lambda_{De} \ll d_e$. The EFE was shown to be part of a sequence of ever longer inertial scale responses adjacent to a magnetic structure that has many of the properties of a slow shock [8], and was located approximately two ion skin depths in front of the low density side of this "slow shock" structure.

In this paper we report on a statistical survey of EFEs accumulated from three years of Polar data. Every few hours of the orbit and hence at a variety of radii, Magnetic Local Times (MLT), and invariant latitudes, Λ, a rapidly sampled "burst" of data was trickled down to the ground in non-real time. The transmitted "burst" was selected onboard the spacecraft as the "best" such event witnessed in the intervening time between "burst" insertions into telemetry. (Although the "burst" data is acquired faster than normal, there is no *a priori* knowledge that these structures are either short scale spatial structures convected over the observer or evolving structures, caught at various stages in their intrinsic time evolution.) Sometimes this strategy did not yield a very large EFE, but quite frequently (258 are surveyed here) this process captured **E**(t) time series that had peak perpendicular electric fields in excess of 100mV/m. For reference the electric field strength in these telemetry bursts are 200-400 times the strength (0.5mV/m) associated with MHD ordered inflow velocities at $0.1V_A$ witnessed in ongoing reconnection layers [2] at Earth's magnetopause. As we develop below, the size of E is not so important in identifying DEFEs as the ratio of the electric force to the magnetic force on a thermal particle; many of the stronger EFEs as indexed by electric field strength alone are relatively ineffective disrupters of gyrotropy because they either occur in strong magnetic field or high thermal speed regimes.

A 700ms portrait of the most frequently occurring "unipolar" type of EFE recovered by such a "burst" strategy is presented in Figure 1. Successive panels depict time profiles of a calibrated (but inferred) density deduced from probe potentials, followed by measured **E** in a cylindrical coordinate system with its z axis along **B**: $|\mathbf{E}_\perp(t)|, \varphi_{\mathbf{E}_\perp}(t)$, and $E_\parallel(t)$. The zero of the phase is the direction of minimum variation of the $\mathbf{E}_\perp$ components. As is typical, this 800Hz "burst" sequence has multiple resolved peaks in $|\mathbf{E}_\perp|$ that exceed 100mV/m, some in excess of 150mV/m; these peaks and the coordinated phase changes suggest (Figures 2, 3) the observations result from a

multiplicity of induced worldline treks across what could be modeled (Appendix1) as a time independent curl free region of enhanced electric fields. In our statistics below the properties of this 700ms of data is treated as one "burst" interval and the peak $|\mathbf{E}_\perp|$ is used statistically to study the properties of all bursts and the plasma regimes where they have been found.

The "unipolar" EFEs' defining property ($E_\perp \approx E$) distinguishes them from the frequently studied [9] solitary "bipolar" structures discovered with the FAST data. When organized in a minimum variance coordinate stystem these structure usually show most of their temporal variation as an excursion of one polarity along a Cartesian axis. The EFE shown n Figure 1 is the "unipolar" burst example with the largest measurable parallel electric fields of any EFE in our 3 year survey (fourth panels of Figures 1, 2). The two traces in the fourth panels of Figure1 and 2 represent the estimates of $E_\parallel$ by two different techniques: (i) component along the direction of minimum variance of electric field for this entire interval (black) and (ii) inner product of **E(t)** and **B(t)** (green) with **B** interpolated to **E**'s much higher time resolution. These two techniques give similar results and both agree that $E_\parallel$ is much smaller in size than $E_\perp$, especially at the E peaks in the series. By contrast "solitary" structures [9] usually have parallel electric fields comparable to the perpendicular ones and also are observed to transit the spacecraft much more rapidly than do the surveyed peaks of our survey. Estimates of solitary speeds with respect to the spacecraft approach the electron thermal speed ($O(2000-4000)$km/s), while the one measured [8] relative speed of a unipolar EFE is well below the local thermal speed, having a speed comparable to MHD wave phase speeds (O(100)km/s). The 11Hz Nyquist condition of the onboard magnetometer data makes the unambiguous detection of weak parallel electric fields difficult in strong electric fields as here; if present in this unipolar data set, parallel components are much smaller than the perpendicular fields.

It suffices for our purposes below to note that these "unipolar" EFE structures are nearly at 90^o to the best estimates of the magnetic field direction; this class of EFE numerically dominates (3:1) the "bursts" recorded in our survey. Within the EFE data set there is a less frequent representation of "bipolar" structures that have comparable perpendicular and parallel fluctuations, but have comparable temporal widths as the "unipolar" EFEs illustrated here. Bipolar structures got their name from their bipolar appearance in a minimum variance coordinate system. In our attempt to distinguish unipolar EFE with weaker $E_\parallel \ll E_\perp$ from bipolar solitary structures, it should <u>not</u> be construed that the observations imply $E_\parallel \equiv 0$. In particular, the experimental determination that $E_\parallel$ is small, measurable or non-existent are three categories. We have stated that the parallel electric field is typically small, if measurable, at EFE unipolar structures, that is, not large. Observationally, such results cannot unequivocally imply that $E_\parallel \equiv 0$.

Even within the 700ms EFE burst in Figure 1, there are many resolved peaks in the intensity of $|\mathbf{E}_\perp|$ that are usually accompanied by a local 20-30% depression in the density. The intensity of E often varies in concert with the phase of this field in the plane perpendicular to $\mathbf{B}$. Subintervals where the phase of $\mathbf{E}_\perp$ is within 20^o of zero are highlighted in cyan in this and Figure 1 and recur frequently in this interval. Often (but not always) these occur at peaks in electric field strength. Centered on 375ms the electric field vector briefly, but smoothly, reorients itself to 180^o from that of many of the peaks in this interval. In this interval the direction of $\mathbf{E}_\perp$ in this EFE is strongly

organized along $\varphi_{E_\perp} = 0, \pi$, an unlikely happenstance if the structures were truly time dependent rather than spatially ordered.

Four lettered intervals in Figure 1 of the many varieties of such coordinated variations are magnified in successive columns in Figure 2. Column D provides an example where the density depression does not occur at the electric field peak, while those in A-C do. The density depressions may reflect structures in electron pressure required to balance varying electric pressure from the stress tensor when the magnetic pressure varies little. Whether EFE are d_e or λ_{De} in scale, ion pressure variations could not compensate for such variations of $\mathbf{EE}/4\pi$.

A candidate time stationary first model of the EFE approximates it (cf Appendix 1) with a structure that depends on at least two spatial coordinates, since otherwise a sheared perpendicular electric field can not be grossly curl free/electrostatic. We emphasize that the modeling of this layer without explicit consideration of the weak $E_\parallel(x, y)$ is an attempt to model the variations of the best measured (perpendicular) components of **E**; to make its point this modeling does nor require that $E_\parallel$ has any numerical profile, that it is constant, that it vanishes identically or is varying in space or not.. Isocontours of the electrical potential (that determines $\mathbf{E}_\perp$) for such a model are indicated in the upper left hand panel of Figure 3. A range of relative motions of the spacecraft and the layer have been used to determine the observer's "worldline" indicated by different colors in this panel. Free parameters in the model (discussed in the appendix) are the relative scale of the width of the unidirectional EFE to the scale of transition into it, the shape of the observer's spatial path across it and the electric strength enhancement realized by the EFE.

The curl free character of the strongest components of the modeled unipolar EFE ensures that there are strong correlations (as in the data) between rotational features in the phase of $\mathbf{E}_\perp$ and its modulus as exhibited in the remaining columns of Figure 3. The two graphs in each successive column in Figure 3 depict the observer's record (upper) of phase variations and (lower) electric field intensity along their world line; their time series are color coded to agree with that of their worldline indicated in the upper left hand panel of the same Figure. These panels show that the order and sign of phase rotations depends on where and in what order the observer's wordline crosses the EFE region $0 \le x \le 1$ and precisely how many times the world line traverses the transitional E layers $x < 0$; $x > 1$ where the reorientation occurs and further intensification can occur. Isolated intensity spikes occur at the edges of the modeled EFE when the transition/width scale $\delta / L \ll 1$, while smoother, wider enhancements with less contrast occur when this ratio exceeds unity. This modeling also indicates that there may only be "one" resolved strongest peak intensity in an EFE region occurring in the region of weak sheer (panel I or cyan peaks in Figure 1 when $\phi_{E_\perp} \simeq 0$) or with multiple peaks at strong angular sheer (panel II and Figure 2A) and that egress and ingress may be accompanied by opposite or same signs of rotation (II vs III). Different worldliness can cause the time profiles of $E_\perp$ to have multiple or single minimaxes without implying underlying intrinsic time dependence. Among the rich diversity of possible transits of the same spatial structure are those (panels IV) where there may be 4 or more reorientations in $\varphi_{\mathbf{E}_\perp}$. Shorter intervals within the 700ms "burst" in the columns of Figure 2 can be reconciled with such a model for their existence. A single layer traversed in all the manners indicated by the colored paths in the upper left hand panel would leave a characteristic phase portrait of the layer as suggested in the lower left subpanel of Figure 3. The union of all

points in the upper left hand panel of Figure 3 would "paint" the entire interior of this phase portrait's bounding region of the lower left hand panel of Figure 3. The short telemetry burst illustrated in Figure 1 is most likely a collection of modeled layers with their common plane perpendicular to the magnetic field and their mean directions $<\mathbf{E}_\perp>$ essentially collinear, since the bursts "phase" portrait is not as simple as a filled in version of that in the lower left hand panel of Figure 3. This is also reinforced by the 180^o reversal at 375ms in Figure 1. Using a model from the Appendix with at least two coplanar curl free layers with antiparallel $\mathbf{E}_\perp$ enhanced layers would be required to model the entire snapshot from this "burst".

We develop next the plasma physical arguments for the size of a "disruptive" or demagnetizing EFE (DEFE), a possible candidate for causing non-gyrotropic modifications to the electron pressure tensor. After sorting events as motivated by the plasma parameters of the theory we organize the geophysical locales of all EFEs and DEFEs.

B. When is an EFE Disruptive?

If **E** and **B** are modeled as time independent, are smooth and slowly varying on the spatial scale of the electron gyroradius, there is no net gain of kinetic energy after averaging over a gyroperiod. (We have shown in the previous section that the data are consistent with spatial, time independent structures, whose time variation in the data records are likely induced by the relative motions of a simple spatial structure. For the remainder we proceed on the presumption that these structures are not intrinsically time dependent.) By contrast, narrow EFEs with scales smaller than the thermal electron's gyroradius can preferentially change the energy of electrons in a manner that will depend on the gyrophase of the electrons as they encounter the narrow region of strong electric field. Figure 4 summarizes the results of tracing collisionless orbits through a curl free EFE whose components lie in the plane of the Figure but are perpendicular to **B**

and is ρ_e in width. We have used Liouville's theorem, the potential structure summarized in the Appendix 1, and have assumed that the velocity distribution function is a generalized Lorentzian ($\kappa = 4$) function of $|v_\perp|$ in Figure 4(C). To illustrate the disruptive character of short scale **E**'s, we have ignored any parallel electric field that may be present, have chosen $v_\parallel = 0$, and reduced the phase space accordingly. The contours in this two dimensional phase space in 4(A), 4(C) illustrate the geometry of level surfaces of the velocity distribution function at all speeds, and gyrophases at pitch angles of $\theta = \pi/2$. The surface is color coded with the same color for each half decade change in the phase space density. Points at every five degrees of gyrophase were mapped from inside the black circle at $10w_e$ in Figure 4(A) to their location in the distribution in Figure 4(C); the spatial locales of Figure 4(A),(B) are in uniform orthogonal electric and magnetic fields of the same size and orientation and, hence drift speeds, $\mathbf{U}_{ExB}$. In steady state Liouville's theorem states that the "color" of $f(\mathbf{v}_1 - \mathbf{U}_{ExB}, x_1)$ is the same as the "color" of $f(\mathbf{v}_2 - \mathbf{U}_{ExB}, x_2)$ provided the equations of motion connect $\{\mathbf{v}_1, \mathbf{x}_1\} \leftrightarrow \{\mathbf{v}_2, \mathbf{x}_2\}$. In this format a distribution function that is gyrotropic has isocontours that are concentric circles as seen at all speeds in Figure 4(C). The colors of the mapped distribution in 4(A) are clearly not cylindrically symmetric even though they represent the Liouville image of a cylindrical distribution

function in a time independent force field. Different gyrophases sometimes have different, non-adiabatic, access across the layer, creating deformations of the level surfaces f. The concentric isocontours of 4(C) are disrupted in 4(A), especially in the vicinity of $-45^o < \Phi_w < 45^o$ and precisely in the speed range to significantly influence the pressure tensor elements. (Since the pressure tensor is essentially dominated by 2-5 thermal speed particles, no (arduous) mappings were attempted for velocities outside the 10 thermal speed black circle in Figure 4(A). In fact some attempted mappings inside the black circle were not successful either; these portions of the phase space show up as white adjacent to colors while still bordering the black circle beyond which no maps were attempted. These regions were near the highest speeds attempted in the above mentioned phase angle regime were strong deformations of successful maps are registered in Figure 4(A).)

Given this motivation we attempt to discover the relationship between the strength of the $E_\perp$ in the EFE and the thickness of the layer in terms of other plasma parameters, to ascertain if the EFEs in the present Polar experimental survey are sufficiently vigorous to assist collisionless reconnection by disrupting the gyrotropy of the electron pressure tensor as has occurred in our controlled mapping illustrated in Figure 4.

C. A Lower Bound for "Strong" EFE:

Of the "unipolar" EFEs reported, a substantial part (if not all) of **E** is perpendicular to the magnetic field. As an initial basis for making our estimates we assume that $\mathbf{E}\bullet\mathbf{B} = 0$ (as in Figure 3,4) and that the electron's prehistory conditions it to be near a turning orbit at one side of the EFE, with the tangent of its unperturbed gyro orbit collinear with **E**. We adopt the notation $\rho_e = m\varpi c/(eB)$ for the gyroradius of the most probable electron with

$$\varpi \ni \frac{d}{dv}\left(f(v)v^2 \right)|_\varpi = 0 \,. \tag{1}$$

For a Maxwellian distribution $\varpi = w_e = \sqrt{2kT_e/m_e}$. We retain the definition of $w_e \equiv \sqrt{2kT_e/m_e}$ where T_e is the related to the trace of the pressure tensor as found by averaging over the observed velocity distribution. For the non-thermal kappa distribution function possessing moment temperature T_e the speed of the most probable electron is

$$\varpi(\kappa) = w_e\sqrt{(2\kappa-3)/(2\kappa)}\,; \tag{2}$$

As $\kappa \to \infty$ the kappa function becomes a Maxwellian and, correctly, $\varpi(\kappa \to \infty) = w_e$.

For a particle of general gyroradius $\rho(\varepsilon) = \varepsilon\rho_e$ the longest path L along the uniform **E** assumed inside the EFE of width $\Delta x = a\rho_e$ is

$$L(a,\varepsilon,\rho_e) = 2\rho_e\sqrt{a(2\varepsilon - a)} \tag{3}$$

$$L(2\varepsilon < a) = 0 \tag{4}$$

The net path length in (3) vanishes exactly whenever (4) the particle's gyro orbit is completely within the EFE, suffering no net energy change while **E**x**B** drifting there. (This is an approximation, since it fails to consider the transition layer between the EFE and its surroundings and any variation of E within the EFE. Also approximate in (3) is the assumption that the particle speed (as for electrons) is large compared to their electric drift speed.)

If the electron fluid's average displacement along the electric field were $< L >_v$, a uniaxial increment to the pressure tensor of the form

$$\Delta(\hat{\mathbf{E}}\bullet\mathbf{P}\bullet\hat{\mathbf{E}}) = neE < L >_{\mathrm{v}} \tag{5}$$

would be realized. If this increment were comparable to the pressure tensor eigenvalues, this interaction with the electric field should be considered disruptive. Thus, if

$$\Delta(\hat{\mathbf{E}}\bullet\mathbf{P}\bullet\hat{\mathbf{E}}) = \frac{\zeta}{2} nkT_e \tag{6}$$

with $\zeta = \mathrm{O}(1)$, we have arrived at a prescription for a "disruptive" EFE, hereafter denoted a DEFE:

$$\mathrm{E}^* = \frac{\zeta kT_e}{2e < L >_{\mathrm{v}}} \tag{7}$$

Next we properly average L over all gyroradii to show how $E^*(a)$ would depend on a. Real plasmas have a range of gyroradii and pitch angles. To account for this (while still retaining our initial approximation) we must average the length (3) along $\mathbf{E}$ over the relevant ambient electron velocity distribution. We define the dimensionless length

$$\Im(a) \equiv \frac{< L(\mathrm{v}_{\perp}, a, f(\mathrm{v})) >_{\mathbf{v}}}{2\rho_e(\varpi)} \tag{8}$$

where $\varepsilon = \mathrm{v}\sin\theta/\varpi$, θ is the pitch angle and v the speed of the particles. The average for $\Im(a)$ becomes:

$$\Im(a) = \frac{\sqrt{a}\int_0^{\pi/2} d\theta \sin\theta \int_{a/(2\sin\theta)}^{\infty} dx x^2 \sqrt{2x\sin\theta - a}\, f(x^2)}{\int_0^{\infty} dx x^2 f(x^2)} \tag{9}$$

independent of the local density. Only the quadratic speed dependence of f has been retained in (9), where the variable $x \equiv \mathrm{v}/\varpi$. Observed PDF's for electrons in space plasmas depend on the components of the velocity (either through convection, thermal anisotropy or skew); however, in the typically occurring ultra-subsonic limit the bulk speed shifts and anisotropy have been initially ignored, leaving conduction skews to keep f from being a symmetric function of speed. Even in simulations of reconnection layers the electron fluid motion only achieves bulk speeds of $U_e \leq (3-4)V_a \ll w_e$. By observations the conduction skews in space plasmas are asymmetries at speeds well above ϖ that we ignore in these first estimates. Accordingly, (9) has been evaluated numerically as if the bulk speed, anisotropy and skew were zero. Using (9) we can now rewrite (7) in the form we desire:

$$\mathrm{E}^*(a, w_e, B) = \frac{\zeta kT_e}{4e\rho_e(\varpi)\Im(a)} = \zeta B \frac{w_e}{c8\Im(a)} \sqrt{\frac{2\kappa}{2\kappa - 3}} = B\frac{v^*(a)}{c} \tag{10}$$

Equation (10) shows that a DEFE is expected when the two parts of the Lorentz force are balanced for a particle of a speed $v^*(a)$ that depends on the thickness of the EFE. The factor involving κ accounts for the differences between increasing the entire pressure tensor element (7) by a fixed fraction and describing all the gyromechanics in terms of the speed ϖ (2) associated with the most frequently occurring member of the PDFs. The special speed is

$$v^*(a, w_e) = \zeta w_e / (8\Im(a))\sqrt{2\kappa/(2\kappa - 3)}\,. \tag{11}$$

It, and hence the threshold E^*/B ratio, are expected to be a strong *increasing* function of the spatial thickness of the EFE.

An alternate way to look at (10) and (11) using (2) and (6) involves forming the ratio between the electric and magnetic force ($\Gamma \equiv cE_{\perp/}/(\varpi B)$ to see that the stronger the Lorentz force ratio, the larger is the separation of perpendicular

$$\Gamma = \zeta(8\Im(a))^{-1} \tag{12}$$

eigenvalues for a given thickness a of the layer.

Figure 5 illustrates the log-log variation of the dimensionless length $\Im(a)$ for Maxwellian and Kappa ($\kappa = 4$) velocity PDFs of equal ϖ as a function of EFE thickness, a. The principal feature of these curves is that EFEs of width comparable to the thermal electron gyroradius produce the longest, PDF averaged, effective lengths along the electric field and thus produce the lowest expected thresholds for $E_\perp^*$ (Figure 6) in a given magnetic field. More quantitatively, the maxima of $\Im$ (horizontal dotted lines) occur at thickness $a = 0.76, 0.94$, for $\kappa = \infty, 4$, respectively. For the geophysical data to be shown below, in situ measurements of observed PDFs are *not* Maxwellian, and values of $\kappa \simeq 4$ are common in the literature. Accordingly, for a fixed magnetic field strength the thickness of these structures at minimum E^* threshold would be very close to $\Delta x \simeq \rho_e(\varpi)$, where we reemphasize that this gyroradius is computed with the speed ϖ of the most frequently occurring particle in the PDF.

A shallow reduction in $\Im$ occurs for $a < 1$ EFEs. Radically shorter $< L >_{\mathrm{v}}$ are in evidence (Figure 5) for thicker (a>2) EFEs. When $a > 1$, more and more of the thermal distribution function becomes guiding center ordered with gyro-orbits fully inside the EFE. Those parts of the velocity distribution (in our idealized estimate) suffer no net displacement along the electric field and are not energized, but simply ExB drift. The number n_{acc} of particles in a Maxwellian PDF that undergo any net displacement along **E** while traversing the layer decreases like

$$\frac{n_{\mathrm{ac}}}{n}\Big|_{a \gg 2} \simeq \frac{a}{\sqrt{\pi}} \exp\left(-\frac{a^2}{4}\right), \tag{13}$$

falling rapidly as a increases, but at a rate that would depend, as here, on the energy dependence of the PDF of the plasma at suprathermal speeds. As shown in Figure 5 $\Im(a)$ is particularly sensitive for a > 1 to the ambient PDF. Frequently a generalized Lorentzian is used to characterize observed distribution functions in the magnetosphere; this distribution is also called the Kappa distribution [10,11] and has the form

$$f_\kappa(\mathrm{v}) = \frac{nA_\kappa}{\pi^{3/2}\varpi^3}\left(1 + \frac{\mathrm{v}^2}{\kappa\varpi^2}\right)^{-(\kappa+1)}. \tag{14}$$

where n is the density. Consistent with our earlier definition ϖ is the speed of the most frequently occurring particle in this PDF for *any* value of κ. For this reason we have averaged L over Maxwellian and Kappa ($\kappa = 4$) PDFs of the same ϖ and density to arrive at the two curves in Figure 5 and 6. Since $\Im(a)$ reflects the displacement along **E** of

all the particles with L > 0 averaged over *all* the particles, it is strongly reduced when $a > 1$. To still acquire the same "disruptive" energy increment, $nk_B T_e/2$, to the pressure tensor (where n is the total density), the reduced pool of unmagnetized particles must encounter ever larger electric fields to acquire the same fiducial change to the pressure. For a given magnetic field strength and disruption ζ to the two perpendicular pressure eigenvalues the threshold electric field $E_\perp^*(a)$ increases strongly (Figure 6) as a exceeds unity (EFE gets thicker than the thermal gyroradius scale) and has a strong dependence on the PDF.

The shortest scale layers known in the solar wind are those associated with shock waves with transition scale lengths $\Delta x \simeq 10\rho_e$ [12]. For such a wide(!) layer the underlying perpendicular electric field becomes demagnetizing with a threshold electric field $E_\perp^*(10)$ *thousands* of times larger than suggested by equation (7) based on $E_\perp^*(1)$. This would correspond to electric drifts hundreds of time in excess of the electron thermal velocity, which do not occur, as the largest solar wind speed on record is 2400km/s. Thus the present analysis does *not* suggest that every MHD flow will make non-gyrotropic electron pressure tensors. It is the shortness of posited scale of the EFE that lowers the threshold so drastically for pressure tensor disruption.

For EFE layers n the vicinity of a=1 in Figures 5 and 6 there is no substantial difference in the prediction of the lower bound for $E_\perp^*$ (from (12) assuming given B) when averaging over either PDF with the same ϖ. Using the velocity space weighted average $\Im(a)$, a more precise *lower limit,* $E^*(a)$, for the "disruptive" electric field strength may be determined. In terms of separate observables the DEFE satisfies the lower bound inequalities

$$\frac{E}{B} \geq \frac{w_e \zeta}{8\Im(a)c} \equiv \frac{E^*(a)}{B} \tag{15}$$

$$\frac{E}{B} \geq 0.159\zeta \frac{w_e}{c} \equiv \frac{E^*(a=0.75)}{B} \quad \textit{Maxwellian} \tag{16}$$

$$\frac{E}{B} \geq 0.109\zeta \frac{w_e}{c} \equiv \frac{E^*(a=0.93)}{B} \quad \kappa = 4 \tag{17}$$

To show the effects of a proper velocity space averaging of (3) an estimate of the coefficient in (15) using (3) at the peak of the Maxwellian pressure integrand determines a value of 0.91.

Restating (7) in terms of the suitably averaged length we finally arrive at our lower bound formula for DEFE:

$$\mathrm{E}^*(a) = \frac{\zeta}{\Im(a)} \frac{kT_e}{4e\rho_e}. \tag{18}$$

and (17) in terms of the Lorentz force fraction is

$$\Gamma_{DEFE} \geq 0.109\zeta \tag{19}$$

Noting from Figure 5 that at its maximum $\Im \simeq 0.9$, the disruptive electric field threshold for a DEFE corresponds to electrical potentials across the most probable particle's gyroradius that is of the order of one quarter the electron temperature in eV.

II. DATA ORGANIZATION

The theoretical inequality (15) is evaluated in Figure 7 using the observed DC electric [13], magnetic field [14], and plasma data [15]. The lower bound of E^*/B is determined by the local thermal speed of the electrons from the ratio of the trace of the pressure tensor and the density

$$T_e = \frac{\mathrm{Tr}}{3nk_B}\iiint d^3\mathrm{v} f_e(\mathbf{v}) m(\mathbf{v}-\mathbf{U})(\mathbf{v}-\mathbf{U}) \qquad (20)$$

as numerically determined [15] from the observed velocity distribution, $f_e(\mathbf{v})$, of electrons corrected for measured spacecraft floating potentials [16] and dynamic pressures associated with the fluid's bulk velocity, $\mathbf{U}$. All EFEs in our 3 year survey are depicted in Figure 7 at observed coordinates $(w_e/c, E_\perp/B)$, using red (blue) symbols for uni(bi)-polar events. Samples in the survey were found ranging over 4 orders of magnitude of field ratios and a factor of 30 in the relativistic factor, w_e/c.

A. Overview of EFE Events in Theory Framework

The green and cyan dashed lines in Figure 7 correspond to the Maxwellian and $\kappa = 4$ values for $\Im$, given by the coefficients in equations (16-17), respectively. A very large fraction 75% of the EFEs are observed with electric field strengths *below* the cyan dashed lower theoretical bound. Accordingly, three quarters of the EFEs are suggested to be unable to cause departures from gyrotropy.

Combining all fields and particle contributions to the relation of Equation (15) we have binned in Figure 8 the dimensionless observed ratio Γ of the electric force to the magnetic force on a mean energy electron in the EFEs in equal logarithmic intervals. Separate histograms reflect percentages of occurrence within a given class of events. The observed distributions of Γ for the bipolar (unipolar) events are in blue (red), respectively. The composite distribution of all events in dashed black reveals a sharp "edge" in the vicinity of $\Gamma_{edge} = 0.1$. This empirical "edge" in the composite EFE set is actually caused by the "edge" in the overpoweringly dominant unipolar (red) EFE group. It should be noted that the location of this empirical edge is close to that theoretically suggested by the vertical green and cyan dashed lines based on Equations 16,17, respectively. Recalling that those edges were derived on the presumption that $\zeta \simeq 1$, the empirical edge at $\Gamma_{\mathrm{obs}} = 0.112 \pm .012$ has a bin width ambiguity of 12% and could easily be made identical with that suggested from the Kappa averaged value of 0.109 in (17). To be conservative in what follows we present results for events that exceed the $\zeta = 1$ thresold. The observed values of Γ for most EFEs are below the cyan theoretical lower bound of $\Gamma = 0.109\zeta$, relevant for the frequently occurring Kappa averaged value of $\Im(a = .93)$ used in (17). By contrast the bipolar group of EFEs is peaked at $\bar{\Gamma}_{bi} \simeq 0.1\Gamma_{edge}$ and well away from the theoretically "disruptive" size suggested by the vertical dashed lines. As a group, the bipolar events are capable of $\zeta_{\mathrm{bi}} \simeq 0.1$ levels of disruption ($\sim 5\%$) to the pressure tensor element along **E**, a full order of magnitude weaker than the mode of the unipolar group. As a group the bipolar events are not typically strong enough to demagnetize electrons as dramatically

as the unipolar events. By contrast the mode of the unipolar group has $\ddot{\Gamma}_{uni} \simeq \Gamma_{edge}$ and a statistically significant population well above Γ_{edge} that are candidates for disruption of gyrotropy (DEFEs). As normalized percentages of their overall occurrence in the sample, the unipolar DEFEs are found 2.5 times more frequently than the bipolar population above their local E* lower bound.

The sharp drop at $\Gamma \simeq \Gamma_{edge}$ in Figure 8 in the vicinity of the numerical values estimated in equation (16)-(17) demonstrates (a) that those theoretical estimates are reasonable, predicting a strong change in occupancy in the correct vicinity, and (b) that EFE events are generally unable to disrupt the electron pressure tensor. However, a small but significant cadre, 39 (15.3%), of the EFE are suggested by this approach to be capable of locally, and unequivocally disrupting the cylindrical symmetry of the electron pressure tensor. One caveat with this conclusion is our assumption that all EFE were assumed to be sampled under the optimal conditions, namely $a \simeq 1$ for our theoretical Γ_{edge} estimates for the location of the vertical lines via (16, 17) in Figure 8. (In Figure 6 it was shown that the bound for causing departures from gyrotropy is a function of the unknown dimensionless width a of the EFE region, and that the minimum for this disruptive bound is in the vicinity of $a \approx 1$. This bound for E^* can easily be raised (so that all measured EFEs are harmless to gyrotropy) by separately tailoring the surmised EFEs thickness for each event, but generally requiring a > 1 to raise the theoretical floor for non-gyrotropic havoc in such a way that no event would disrupt the pressure tensor's cylindrical symmetry.) More carefully, then, $\Gamma > .109\zeta \simeq 0.1$ EFEs should be viewed as *candidate* DEFEs, provided $a \sim 1$ could be established for them. We address the issue of the spatial scale of the EFEs in five ways: (i) the β_e distribution, (ii) the λ_{De} / ρ_e distribution, (iii) the known thickness of any of these events, (iv) relevant simulations of separatrix layers, and (v) the geophysical organization of provisionally identified DEFEs based on $a \sim 1$.

B. EFE Organization with β_e

All uni-polar (red) and bi-polar (blue) EFEs are found in either the solid red or blue histograms in Figure 9 that depicts the organization of the electron β_e in the EFEs. The candidate "disruptive" DEFE examples ($a \sim 1$) are indicated by dashed histograms using the same colors. All EFEs were found in $\beta_e \leq 3\times10^{-2}$ plasmas; the modal β_e for the all EFEs is approximately 10^{-4}. Such a β_e regime is inconsistent with the electron gyroradius exceeding the electron skin depth, an expected minimum scale of current layers of the magnetic field since $\rho_e \equiv \beta_e^{1/2} d_e$. However, these histograms are consistent with our premise: the locales of DEFEs are not those of large $\beta_e \gg 1$ regimes where electron skin depth current layers could also provide for demagnetization. Had the EFEs been found in such large β_e regimes, their possible role as an agent in any possible demagnetization would be clouded by the possibility of competition. All EFE events are low $\beta_e \ll 1$. However, all "disruptive" DEFEs occur in a restricted

upper range of this $\beta_e < 3\times10^{-2}$ regime with a modal value in excess of 10^{-3}. We now consider the ratio of the electron Debye length to thermal gyroradius as a possible ordering parameter of the locales where DEFE were found.

C. EFE Organization with λ_{De}/ρ_e

When considering quasi-dc electric fields in a plasma, the electron Debye length provides a natural minimal scale for the electrostatic structures expected in such fields. The abrupt and intense nature of the electric field in the EFE suggests that they may be supported by space charge layers of a few Debye lengths in width [7], a possibility supported by one direct measurements of their scale [8]. We have seen in Figures 3 and 4 above that the spatial width of the EFE plays a role in determining how disturbing such a layer will be for the gyrotropy of the thermal electrons. In particular, if the layer is too thick relative to the thermal gyroradius, then the threshold electric field (cf. Figure 6) would be markedly higher. On the other hand to find an electrostatic structure below the scale of the electron thermal gyroradius is problematic unless the Debye length is locally smaller than the gyroradius. Accordingly we have explored the relative size of the Debye length to the electron's thermal gyroradius at the EFE sites of our survey.

The ratio $\Re$ of the electron Debye length to thermal gyroradius is given by the equivalent expressions:

$$\Re \equiv \frac{\lambda_{De}}{\rho_e} = \frac{\Omega_{ce}}{\omega_{pe}} = \frac{w_e}{c}\beta_e^{-1/2} \qquad (21)$$

As seen in Figure 7, the electron thermal speed regimes of the EFE intervals range between (.003-.1)c. Accordingly, the very lowest β_e regimes exhibited in Figure 9 correspond to plasma regimes where certainly $\Re \gg 1$. The "disruptive" DEFEs have among the largest β_e's of the EFE population, while still satisfying $\beta_e < 0.03$. The distribution of $\Re$ for the demagnetizing subset of both types (all EFE) is shown in the solid (dashed) histogram in Figure 10. The solid DEFE histogram at small values of $\Re$ has $<\Re><1$ and represents a low amplitude "wing" of the entire EFE distribution which has a much higher mean value of $<\Re>>1$. The DEFEs found according to Equation 17 are thus shown to occur in almost all cases in plasmas where $\Re \le 1$. Thus, DEFE events selected by Equation 17 (that does not involve the density) is nearly one-to-one associated with a property that they occur where there exists a natural plasma scale (determined by density) associated with the electric field that is at or beneath that of the electron's thermal gyroscale, $\Re \le 1$. If the uni-polar DEFE have transverse extents Δx that were a few Debye lengths, such structures can easily have $\Delta x \simeq m\lambda_{De} \simeq \rho_e$, with m an order unity number provided as a class $\Re_{DEFE} \le 1$ as illustrated in Figure 10. Conversely, it is hard to imagine striated electric field with scales shorter than λ_{De}; assuming that EFEs cannot go below the Debye length in spatial scale, the thinnest layers with $\Re > 1$ have very large values of a, and much enhanced thresholds for E to be demagnetizing (cf. Figure 6). *For the DEFEs (solid histogram in Figure 10) the threshold estimates made above for* $\Im(a \approx 1)$ *should be consistent for inferring events as demagnetizing.* [On the contrary if these events were found to have had $\Re \gg 1$, there would be no obvious plasma scale available to stratify **E** on a scale below that of ρ_e, contradicting our thesis. Accordingly, our premise is not contradicted by these additional considerations, but strengthened by passing a new test involving more observational constraints.]

D. Measured Spatial Scales of EFE:

The statistical arguments of the preceding paragraphs gain additional credence from the one EFE layer that we have been fortunate to assign/measure spatial scales. The carefully documented [8] event of this class of unipolar

EFE has been "measured" to have an e-folding scale of $7\lambda_{De} \approx \rho_e$, consistent with our premise. The peak electric field strength for that EFE was 150mV/m, the magnetic field strength 70nT and c/w_e=103, yielding an R=.745, making it amongst the strongest DEFE events in this survey. This event occurred on January 31, 2004 and is located in Figure 7 with a black asterisk and in Figure 8 at the position of the downward pointing arrow.

E. Simulations:

In situ observations [2] and full particle simulations [8,17,18] have recently shown that the vicinity of the separatrices are the sites of very strong perpendicular electric fields and also sites of strong departures [8,18] from electron gyrotropy. Three of the simulations report electric layers with scales of the order of ρ_e on the separatrix as well as near the separator. If as a class EFEs were transits of separatrix layers, it would explain their frequent detection along cusp invariant latitudes as illustrated in the next section. EFEs that are not DEFEs could be viewed as layers of strong electric field organized by, caused by, or shed by separatrices, but perhaps no longer strong causative agents of non-ideal behavior along the separatrices. In this picture the DEFEs would be those sites where intense EFEs in the dimensionless sense of (17) are making non-ideal MHD behavior possible, and these are found to be DEFEs by our cataloguing system. The complementary set of EFEs that are not DEFES could then be viewed as locales away from the separator out along separatrices.

F. Geophysical Locales:

The original group of EFEs of our three year survey was found to be distributed over a wide range of geophysical regions of the magnetosphere. The green histograms in Figure 11 illustrate the geophysical locales of all EFEs in the present survey segregated by radial location, R, panel (A), by Magnetic Local Time (MLT), panel (B); by Invariant Latitude, Λ, panel (C); and magnetic latitude, panel (D). In each panel the red (blue) distributions indicate the location of the "disruptive" DEFE unipolar (bipolar) events. The unipolar DEFE events are preferentially found near Polar's apogee beyond $8R_e$, while the 4 "disruptive" EFE bipolar events occurred with no perceptible preference for altitude.

The green histogram in 11(C) demonstrates that *all* EFE events of the survey were localized broadly at cusp invariant latitudes between $65^o \leq \Lambda \leq 82^o$, but at rather wide distribution of magnetic local times, Figure 11(B). (The atmospheric drag induced apsidal precession on the Polar spacecraft only allowed northern hemisphere cusp coverage at the magnetopause in the three year period of this survey.) The unipolar DEFE events are more strongly clustered in Λ than the parent population (cf. Figure 12) , being largely confined between 70-76^o, towards the lower range of the recently resurveyed cusp [20]. The DEFE events occurred preferentially about the magnetic noon-midnight plane, with over 70% of the demagnetizing unipolar EFEs found within ± 4hr of magnetic local noon; another 11% of the demagnetizing population were found within the same displacement of local midnight as illustrated in Figure 11(C). A full 37% of the unipolar DEFEs were found within ± 1 hour of noon MLT, at a level that is 3-4 times the frequency of EFEs in that same time interval. The limited number of "disruptive" bipolar EFE events "are consistent with", but do not independently define, this type of local time distribution. The (MLT, Λ) organization of the EFE (unipolar DEFE) is explicitly organized with black (red) symbols in Figure 12. The blue dashed box in this figure is the recent empirical delineation of the cusp [20].

III. SUMMARY

We have shown that all of the surveyed EFEs of the 3 year Polar survey occur in very low $\beta_e \ll 1$ plasmas. A lower bound for the electric field strength, $E^*(a)$, for "disruptive" DEFE behavior has been derived as a function of DEFE thickness, a (Eqtns 10,15-17). The minimum of this lower bound has been shown to occur in EFEs with thicknesses of order $a = \Delta x / \rho_e \simeq 1$. In order that we find the largest possible number of DEFEs, we have sorted the observed EFEs against this minimum lower bound, assuming a thermal gyroradius thickness for all events; we determine that only a small subset of the EFEs are sufficiently intense to provide "disruptive" perturbations to the pressure tensor of electrons. Almost without exception, the "disruptive" unipolar DEFEs occur in plasma locales where $\lambda_{De} \leq \rho_e$, consistent with the idea that they occur in plasmas with foreseeable electrostatic scales lengths between the electron Debye and thermal gyroradius scales. A recent "strong" DEFE has been analyzed [8] for its geometry and such short scales have been "measured" and the relation of these structures to the attending MHD variations discussed. Recent simulations also reveal narrow thermal gyroradius scale electrostatic layers along the separatrices of modeled collisionless reconnection layers, and that they are capable of producing non-gyrotropic electron pressure tensors [8,18] as have been reported with in situ measurements at other magnetopause layers [2].

The "disruptive" EFEs (DEFEs) were initially categorized using local plasma criteria without knowledge of the geophysical locales where they occurred. Gratifyingly, the DEFE events do occur in geophysical locations (Figure 10) where collisionless magnetic reconnection has long been suspected to occur, but with little direct information of how departures from ideal MHD behavior might be enabled. Both types of "disruptive" EFEs occur preferentially near local noon and midnight, with local noon events comprising over 70% of these events identified without any reference to geophysical locales. The unipolar events show a strong preference for the apogee of the orbit that is near the nominal magnetopause (Figure 10(A)). A slight preference is demonstrated for intermediate northerly magnetic latitudes in Figure 11(D); this organization may not be intrinsic, but a bias of the orbital circumstances when Polar is at local noon MLT and apogee during this interval of its mission.

The "disruptive" unipolar/bipolar DEFEs that exceed the relevant lower bound for E^* are especially attractive candidates for demagnetization of the fluid description of electrons in low β_e plasmas, even if they were shown to occur in the thinnest electron skin depth current layers where they would be considered guiding center ordered *against the variations in the magnetic field*. These DEFE are candidate coherent, and essentially DC agents for demagnetization of the electron fluid in low $\beta_e < 1$ plasmas; as a morphological category they are contrapuntal to the regime of expected demagnetization at high $\beta_e \gg 1$ enabled by well known electron skin depth current channels. It is a distinct possibility that these structures by their Λ organization and occurrence in simulations are part of and are maintained as part of the separatrices of quasi-stationary patterns of collisionless magnetic reconnection [8, 17,and 18].

The detection here of disruptive DEFEs that exceed the threshold condition (17) and Figure 8 should be considered as *prima facie* evidence that *electron* finite Larmor radius FLR effects at such narrow enhancements of the

electric field could coherently enable non-ideal properties required by global observations in real, collisionless, low $\beta_e < 1$ plasmas such as solar flares, machine plasmas, and in planetary magnetospheres.

Acknowledgments: JDS acknowledges data support by S. Li, D. Morgan, and R. Holdaway at U. Iowa. Work was supported under contracts NNG05GC72G and NNG05GC28G at the UC Berkeley and the University of Iowa, respectively.

Appendix: Model for EFEs

The trajectories used to construct Figure 3 were obtained using an assumed curl free electric field of the form

$$\mathbf{E} = \hat{\mathbf{x}}\frac{y}{2\delta}\left(\sec h^2\frac{x}{\delta} - \sec h^2\frac{x-a\rho_e}{\delta}\right) + \hat{\mathbf{y}}\left(E_\infty + \frac{\Delta E}{2}\left(\tanh\frac{x}{\delta} - \tanh\frac{x-a\rho_e}{\delta}\right)\right) \qquad \text{(A1)}$$

assumed to be purely orthogonal to the assumed spatially uniform magnetic field: $\mathbf{B} = B_o\hat{\boldsymbol{z}}$. (It should be noted that this model pertains to the most accurately measured, largest components of E, and by its success in explaining the observables, does not prove that the parallel electric field is uniform, zero, or anything other than small.) The main enhancement in the electric field (ΔE) occurs between $x = (0, a\rho_e)$, while smoothly transitioning back to a smaller values E_∞ on either side of the layer. Values assumed were a=1 and $\delta = .01\rho_e$. The x component is required to produce a potential field of zero curl, and causes thin ribbons of intensified electric fields on the edges of the principal layer to have a pattern of quadrupolar symmetry. Trajectories were integrated using fourth order Runge-Kutta algorithm until the orbit traversed the enhanced E layer and its entire gyro orbit was clear of the non-uniform electric layer. Figure 4 was constructed assuming the $f_e(v_\perp, \phi, v_\parallel = 0, \mathbf{x}_1) = g(v_\perp, E_\infty, B_o)$ to construct $f_e(v_\perp, \phi, \mathbf{x}_2)$ via Liouville's theorem, where $\mathbf{x}_1, \mathbf{x}_2$ are locations on either side of the enhancement of E where $\langle f_e v_\perp d^3v\rangle / \langle f_e d^3v\rangle \equiv cE_\infty / B_o$. The curl free requirements (Cauchy-Riemann conditions) couple with the posited localized form of E_y yields the observed azimuthal patterns upon ingress and egress of the modeled EFE.

REFERENCES:

[**1]** J.D. Scudder, *Space Sci. Rev.* **80**, 235-267 (1997)

[**2**] J.D. Scudder, F.S. Mozer, N. C. Maynard, and C.T. Russell, *J. Geophys. Res.,* **107** (A10), SMP 13-1: SMP 13-38, doi:10.1029/2001JA000126 (2002)

[**3]** V.M. Vasyliunas, *Rev. Geophys. Space Phys*. **13**, 303 (1975)

[**4]** M. Kuznetsova, M. Hesse and D. Winske, *J. Geophys. Res.* **15**, 3799 (2001)

[5] P. Ricci, J.U. Brackbill, W. Daughton, and G. Lapenta, *Phys. of Plasmas* **11**, 8, 4102 (2004)

[**6]** E.N. Parker, *Phys. Rev*. **107**, 924 (1957)

[7] F.S. Mozer, S.D. Bale, J.D. Scudder, *Geophys. Res. Letts.* **31**, 15, CiteID L15802 (2004)

[**8]** J.D. Scudder, Z.W. Ma and F.S. Mozer, Debye length structures in Earth's reconnection layer: observations and simulations, to be submitted, *Phys. of Plasmas*, 2005.

[9] R.E. Ergun, C.W. Carlson, J.P. McFadden, et al., *Phys. Rev. Letts*. **81**, 4, 826 (2001)

[**10] S.** Olbert, in Physics of the Magnetosphere, Dordrecht: Reidel, R.D.L. Carovillano and J. F. McClay eds., Astrophysics and Space Science Library **10**, 641 (1968)

[**11]** V.M. Vasyliunas, 1968, *J. Geophys. Res.* **73**, 2839 (1968)

[12] J.D. Scudder, T.L. Aggson, A. Mangeney, et al., *J. Geophys. Res.* **91**, 11053 (1986)

[13] P. Harvey, F.S. Mozer, D. Pankow, et al., *Space Sci. Rev.* **71,** 1-4, 583 (1995)

[**14]** C.T. Russell, R.C. Snare, J.D. Means, D. Pierce, D. Dearborn, M. Larson, G. Barr, and G. Le, *Space Sci. Rev.* **71**, 1-4, 563 (1995)

[**15]** J.D. Scudder, F. Hunsaker, G. Miller, et al., *Space Sci. Rev*. **71**, 1-4, 459 (1995)

[16] J.D. Scudder, X. Cao, and F.S. Mozer, *J. Geophys. Res.* **105**, 20,957 (2000)

[**17]** P.A. Pritchett, *Phys. Plasma* 12, 062301 (2005)

[**18]** W. Daughton, Private communication, January (2005)

[19] C. Cattell, J. Dombeck, J. Wygant, et al., *J. Geophys. Res.* **110**, A01211, doi:10.1029/2004JA010519 (2005)

[20] X.W. Zhou, C.T. Russell, S.A. Fuselier, and J.D. Scudder**,** *Geophys. Res. Lett*., **3**, 429 (1999)

Figure Captions:

Figure 1. (Color) Example of an EFE using data capture over 700ms acquired on NASA's Polar spacecraft on April 1, 2001, starting at 23:24:56.40164UT. "Burst" of high resolution electric field date collected at 800Hz. From the top, inferred density from probe potentials, magnitude of components of $\mathbf{E}$ perpendicular to **B**, phase angle of $\mathbf{E}_\perp$ relative to the direction of minimum variance of $\mathbf{E}_\perp$, followed by $\mathbf{E}\bullet\hat{\mathbf{B}}$ inferred by two different methods described in the text. Agua shading indicates locales where the phase of $\mathbf{E}_\perp$ goes through zero. Frequently this is also a peak in $\mathbf{E}_\perp$. $E_\parallel$ trace is constructed two different ways: green and black trace described in text. Both methods agree that routinely and at the peaks of $\mathbf{E}_\perp$, that $E_\parallel \ll E_\perp$.

Figure 2. (Color) Four insets from Figure 1 (keyed by corresponding letters), showing the laminar character of the resolved time series and the correlation of the variations of $E_\perp$ with cylindrical phase, and local density variations. Same format as Figure 1.

Figure 3. (Color) Simulation of data acquisition across a planar, modeled curl free electric field pattern for perpendicular $\mathbf{E}_\perp$ in EFE. This model has been introduced to discusss the morphology of the largest (perpendicular to B) components in the EFE. In no way does the model or its use imply or require that $E_\parallel \equiv 0$. Upper left hand panel illustrates the modeled equipotentials and depicts various colored worldlines of hypothetical spacecraft crossings of the EFE. Successive columns of panels illustrate the time profiles of $E_\perp(t)$ and $\varphi_{E_\perp}(t)$, using colors to match those that label the worldlines in upper left hand panel. Lower left hand panel depicts the phase portrait of all observers along the indicated worldliness in upper left hand panel. The union of all points in the upper left hand panel would "paint" the interior of the phase portrait that is presently delineated in lower left hand panel. Such arguments show that the data in individual columns in Figure 2 may be modeled in this way, but that the entire burst cannot be represented by just one such structure as in the upper left hand corner.

Figure 4. (Color) Summary of detailed integrations of equation of motion for electrons (through an EFE as illustrated in inset B) connecting points of observation at two points (A) and (C) well removed from any gradients in **E**. Use has been made of Liouville's theorem. Isocontours are made of velocity space in the equatorial plane with the magnetic field as its pole. Since $\mathbf{E}\bullet\hat{\mathbf{B}} = 0$ phase space is 4-d and all coordinates are resolved here. Velocity distribution at 4(C) is a generalized Lorentzian, Kappa function with $\kappa = 4$, that is gyrotropic – hence the concentric phase space zones. Since the Hamiltonian is time independent the trajectories are time reversible, and the phase space at (A) is constructed by numerically integrating the equations of motion from (A) to the locale of (C) and "painting" the distribution function in (A) accordingly. $\Gamma = 0.1$ at threshold has been assumed. Mapping done at 5^o increments Γ within the black circular border of inset (A). Portions of phase space that are white inside the black circular ring in (A) are locales where connection trajectories could not be found. These regions invariably adjoin phase space regimes reflecting non-gyrotropic access. No phase space matching was attempted outside the black circular border in inset

(A) since the trajectories required too much computer time. Note distortions in that part of velocity space that determine the maximum contribution to the pressure tensor elements.

Figure 5. Velocity spaced averages of dimensionless ratio $\Im(a)$ that determines (14), the net energy per particle available from non-guiding center ordered electron behavior in EFEs with thickness $\Delta x = a\rho_e$. Two velocity PDFs are contrasted with the same density and speed of most probable particle. Note maximum in the vicinity of $a \simeq 1$ and strong sensitivity to the distribution of the phase space with energy.

Figure 6. Theoretical variation of $\Gamma(a) = cE^*(a)/(w_e B\zeta G(\kappa))$ that determines the lower limit threshold electric field $E^*(a)$. The function $G(\kappa) = \left(2\kappa/(2\kappa - 3)\right)^{1/2}$. Since this ratio Γ is determined by $\Im(a)^{-1}$ it has a broad minimum in the vicinity of $a \simeq 1$, while retaining a strong sensitivity to the energy dependence of the phase space distribution of electrons when $a > 2$. The minimum threshold for $\kappa = 4$ occurs at $\Gamma(a = 0.93, \kappa = 4) = 0.11$, while that for the Maxwellian distribution occurs at $\Gamma(a = 0.75, \kappa = \infty) = 0.16$. These two values of Γ set the horizontal dashed lines in this figure and set the locations of the cyan and green lines in Figures 7 and 8.

Figure 7. (Color) E/B vs w_e/c using only observables. Cyan and green dashed lines are theoretical boundaries implied by (15,16). Black asterisk is location in parameter space of only EFE event whose spatial scales have been measured [8].

Figure 8. (Color) Observed distribution of Lorentz force ratio, $\Gamma_{obs} = cE_{\rm obs}/(w_{e,\rm obs} B_{\rm obs})$. Black histogram: all EFE; red: unipolar EFE; blue: dipolar EFE. Vertical dashed green and cyan lines are theoretical values for $\Gamma_{\rm theory}(a = 1)$ determined from Gaussian or Kappa velocity distribution averages reflected in Equations (15),(16), respectively. Asterisk denotes the location of the only EFE event [8] whose spatial scales are known by measurement; it is clearly shown here as a DEFE.

Figure 9. (Color) β_e distribution given by solid histograms for unipolar EFEs (red) bipolar EFEs (blue). Corresponding classes of DEFEs given by dashed histograms with the same colors. EFEs are a very low β_e phenomena.

Figure 10. $\Re = \lambda_{De}/\rho_e$ distribution for DEFEs (solid) all EFEs (dashed).

Figure 11. (Color) Geophysical locales of EFEs: (A) radius in Earth radii; (B) Magnetic Local Time (MLT) hours (noon = 12); (C) Invariant Magnetic Latitude, Λ (degrees); (D) Magnetic Latitude, (degrees). All EFEs in green; unipolar DEFEs (red); and bipolar DEFEs (cyan-aqua).

Figure 12. (Color) MLT- Λ distribution: all EFEs in black; unipolar DEFEs red symbols connected by line segment. Blue dashed box is the recently resurveyed [20] boundary of the Earth's, magnetic cusp in the northern hemisphere. Vertical green dashed lines indicate ±4hr of local noon where DEFEs are preferentially found. Next highest local is local midnight.

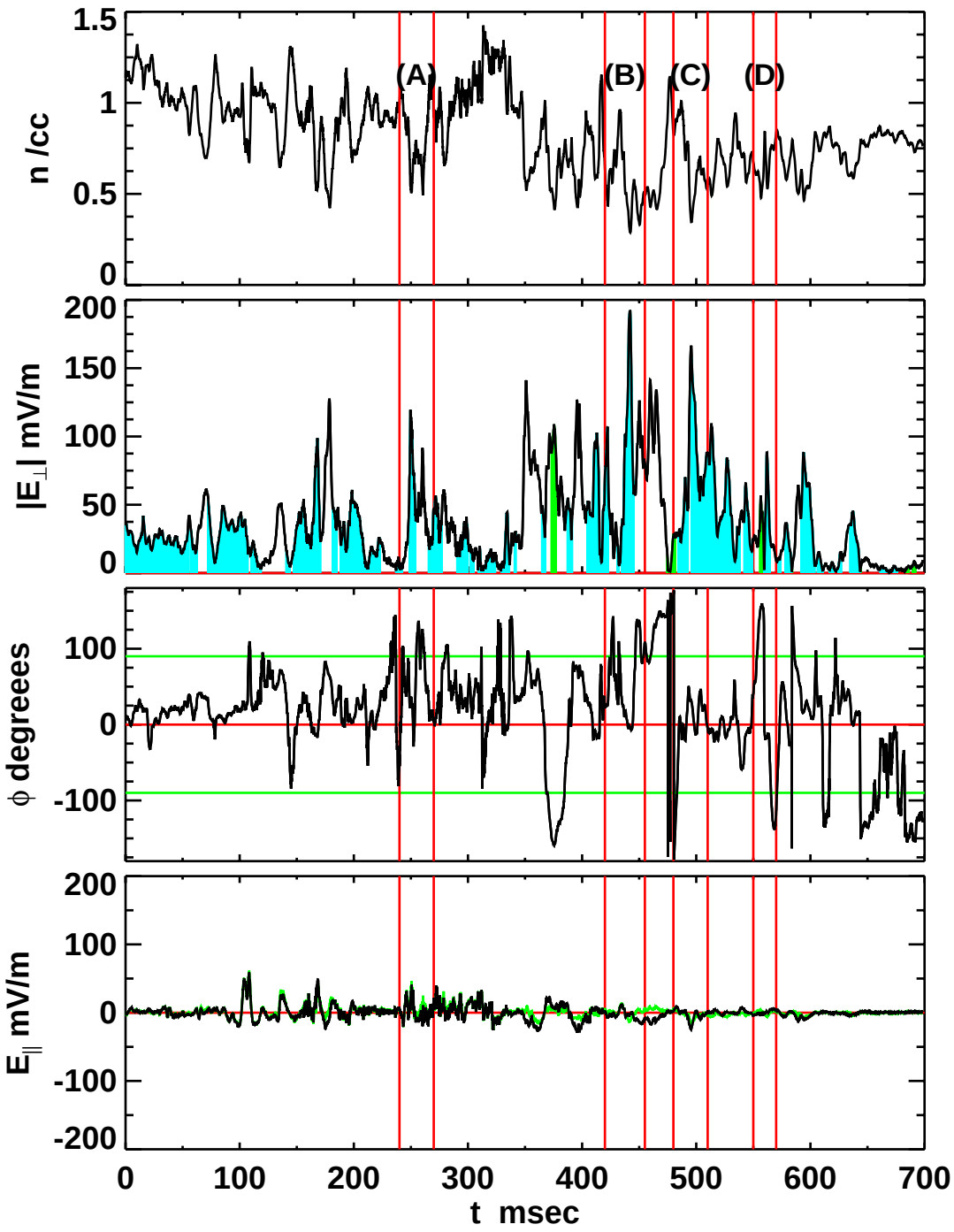
1.5
1
0.5
0
n /cc
(A)
(B)
(C)
(D)
200
150
100
50
0
|E⊥| mV/m
100
0
-100
ϕ degrees
200
100
0
-100
-200
E|| mV/m
0
100
200
300
400
500
600
700
t msec

Figure 1

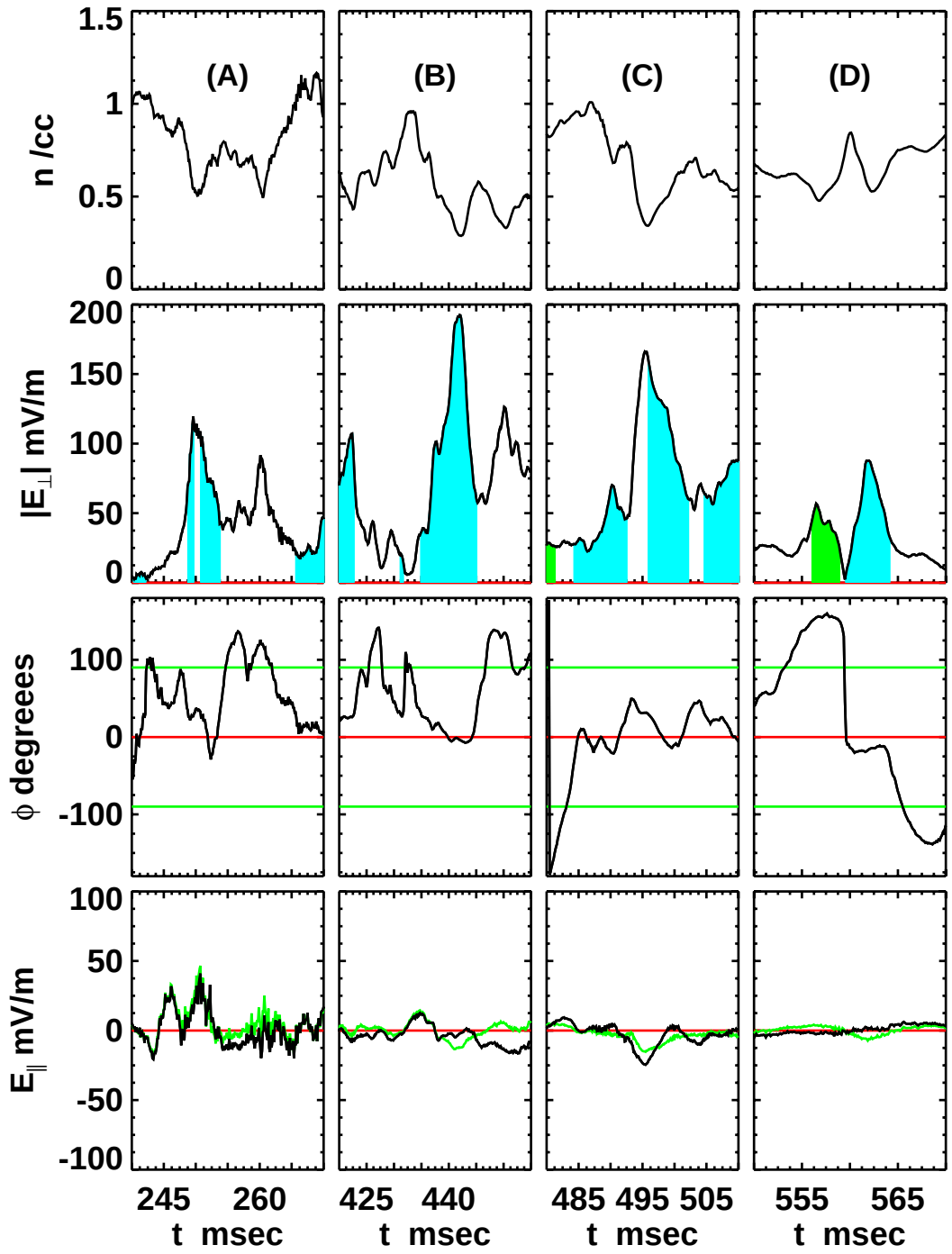
(A)
(B)
(C)
(D)
n /cc
1.5
1
0.5
0
|E⊥| mV/m
200
150
100
50
0
ϕ degrees
100
0
-100
E∥ mV/m
100
50
0
-50
-100
245
260
425
440
485
495
505
555
565
t msec
t msec
t msec
t msec

Figure2

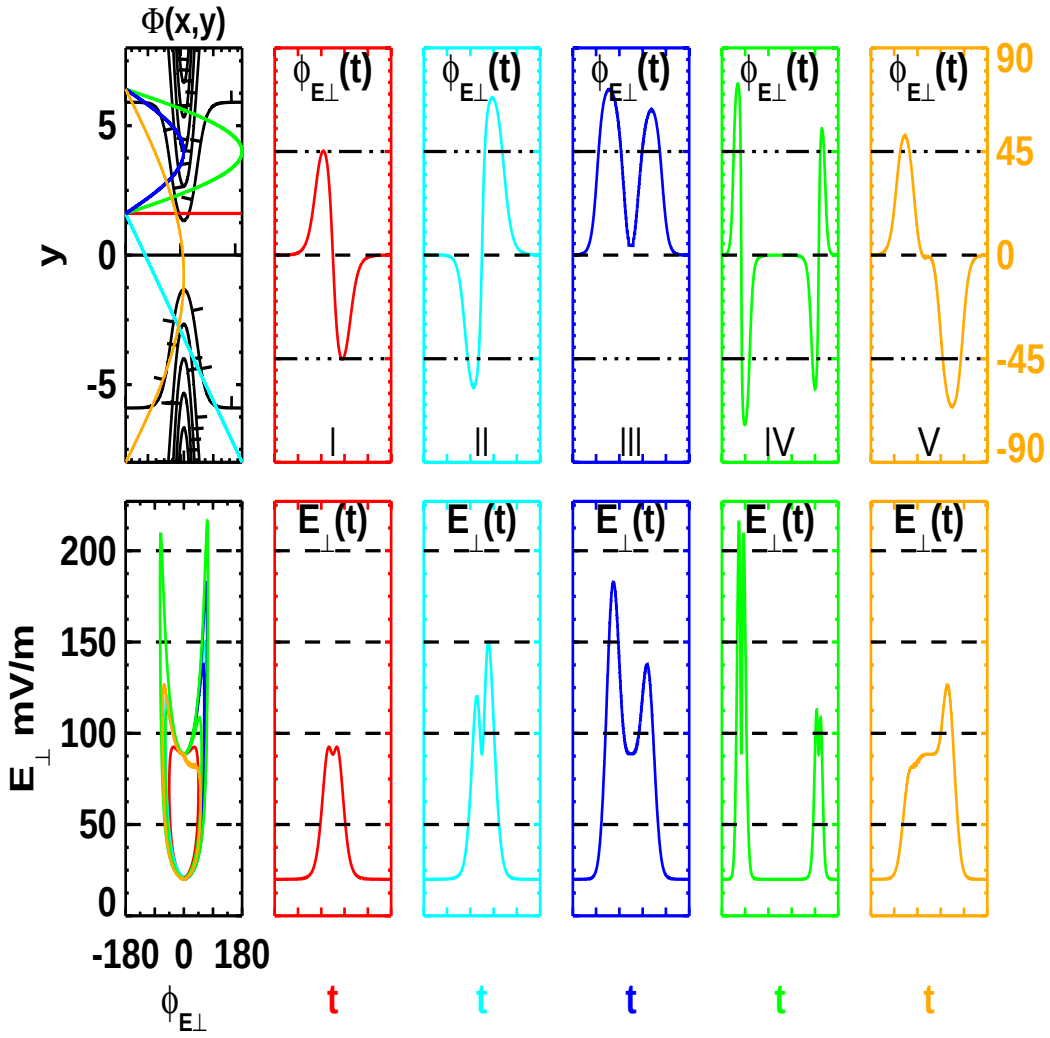

Figure 3

Figure 3

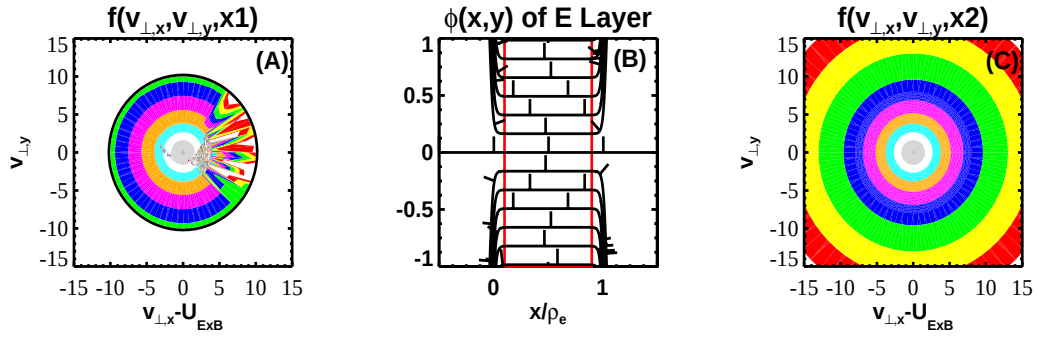

Figure 4

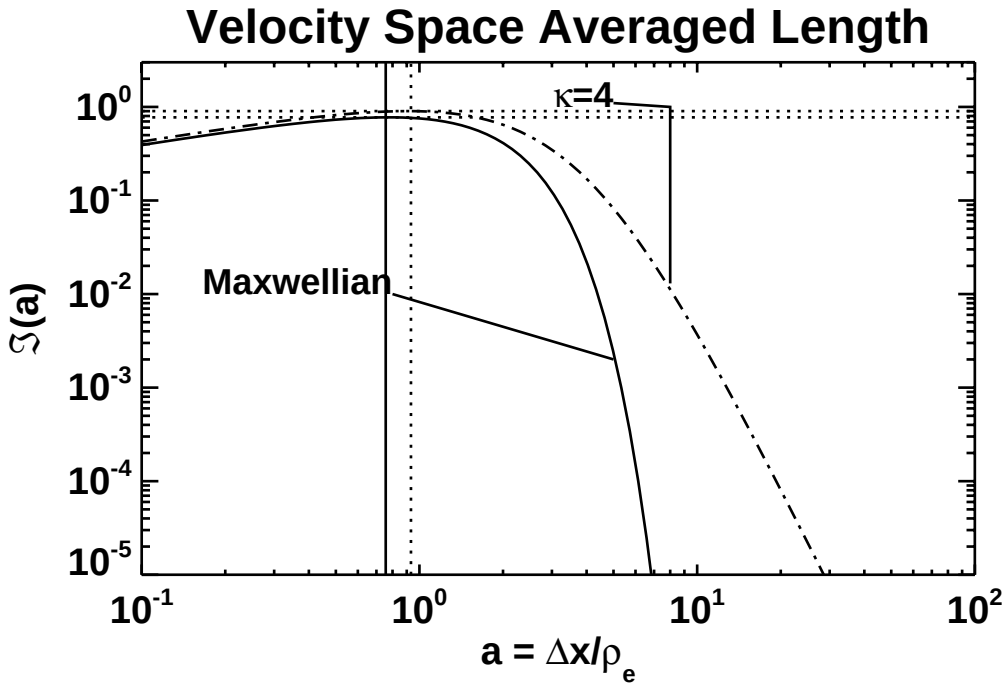
Velocity Space Averaged Length
κ=4
Maxwellian
𝔍(a)
10^0
10^-1
10^-2
10^-3
10^-4
10^-5
10^-1
10^0
10^1
10^2
a = Δx/ρ_e

Figure 5

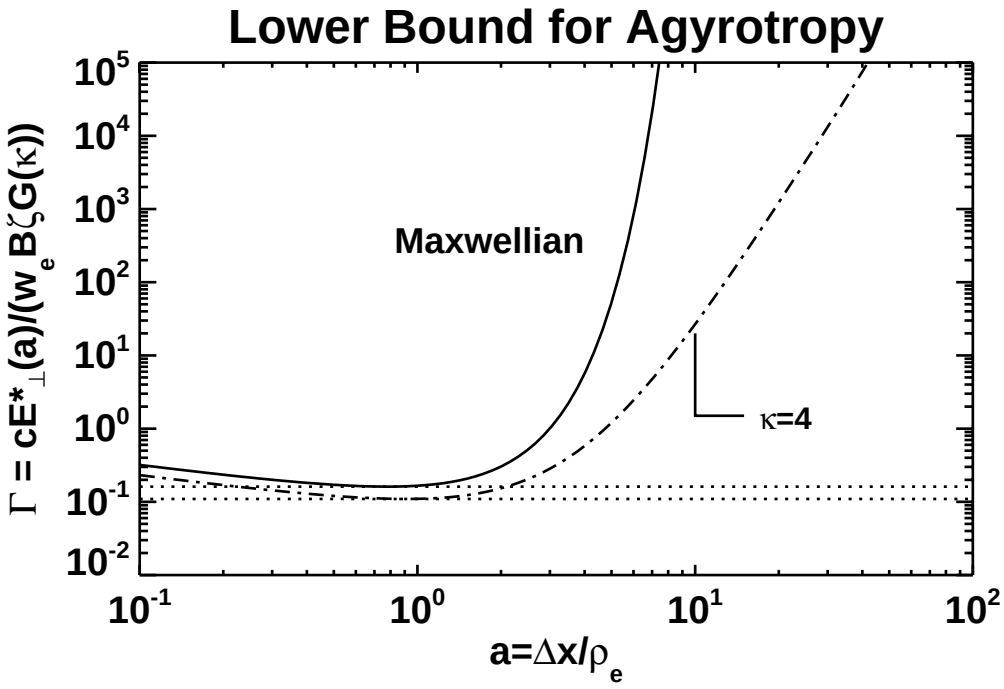
Lower Bound for Agyrotropy
Maxwellian
κ=4
Γ = cE*⊥(a)/(w_e B ζ G(κ))
a=Δx/ρ_e
10^5
10^4
10^3
10^2
10^1
10^0
10^-1
10^-2
10^-1
10^0
10^1
10^2

Figure 6

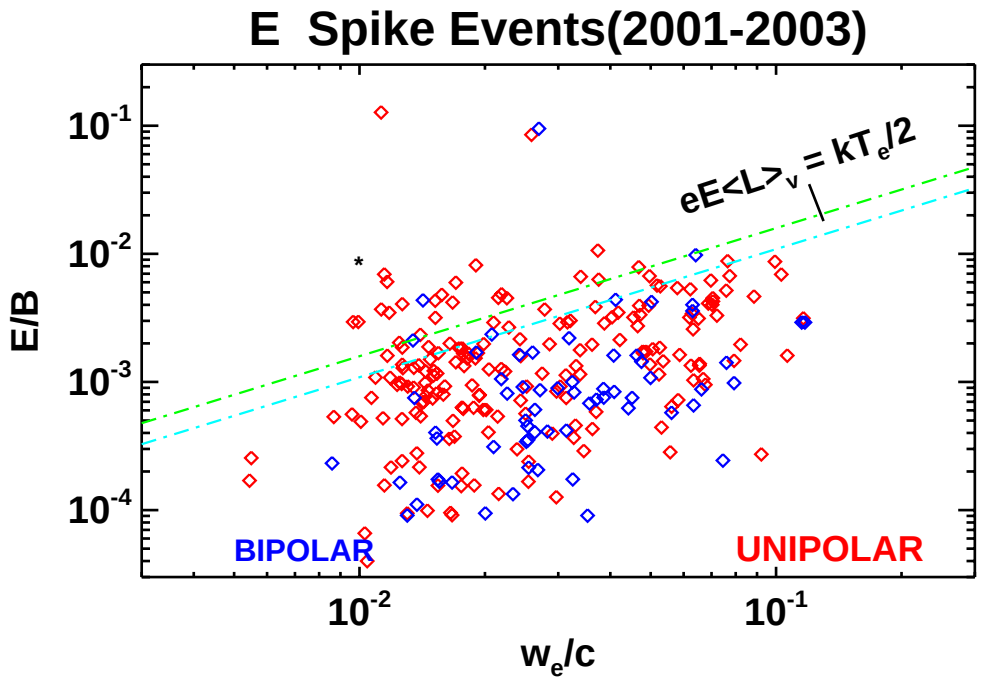
E Spike Events(2001-2003)
E/B
10^{-1}
10^{-2}
10^{-3}
10^{-4}
$eE\langle L\rangle_v = kT_e/2$
BIPOLAR
UNIPOLAR
10^{-2}
10^{-1}
w_e/c

Figure 7

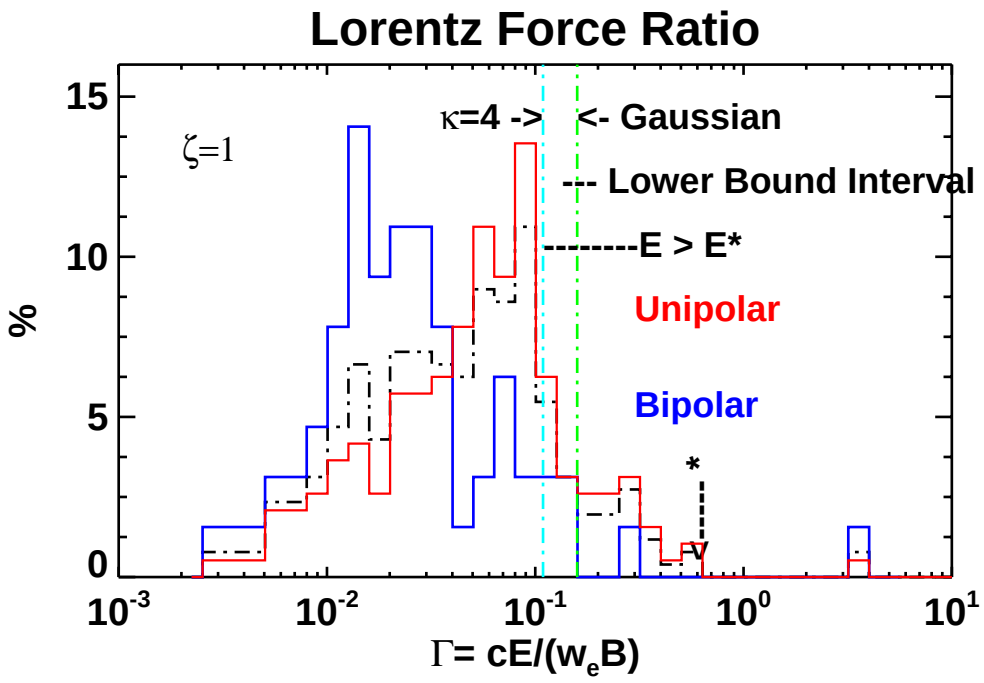
Lorentz Force Ratio
15
10
5
0
%
ζ=1
κ=4 ->
<- Gaussian
--- Lower Bound Interval
--------E > E*
Unipolar
Bipolar
*
10^-3
10^-2
10^-1
10^0
10^1
Γ= cE/(w_eB)

Figure 8

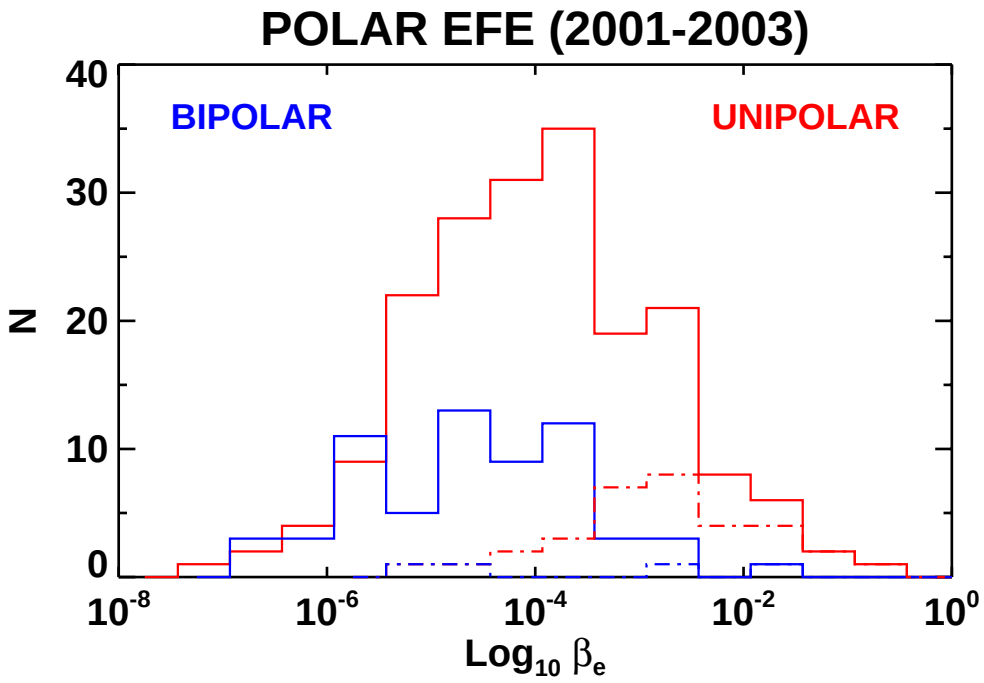
POLAR EFE (2001-2003)
BIPOLAR
UNIPOLAR
N
40
30
20
10
0
10^-8
10^-6
10^-4
10^-2
10^0
Log10 βe

Figure 9

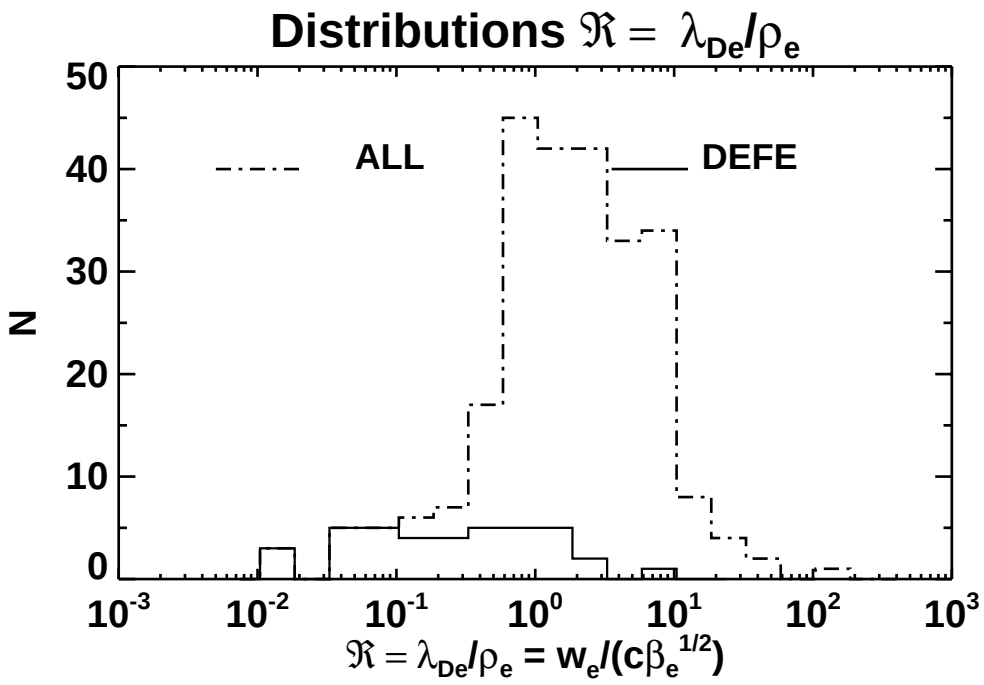
Distributions $\Re = \lambda_{De}/\rho_e$
ALL
DEFE
N
50
40
30
20
10
0
10^{-3}
10^{-2}
10^{-1}
10^{0}
10^{1}
10^{2}
10^{3}
$\Re = \lambda_{De}/\rho_e = w_e/(c\beta_e^{1/2})$

Figure 10

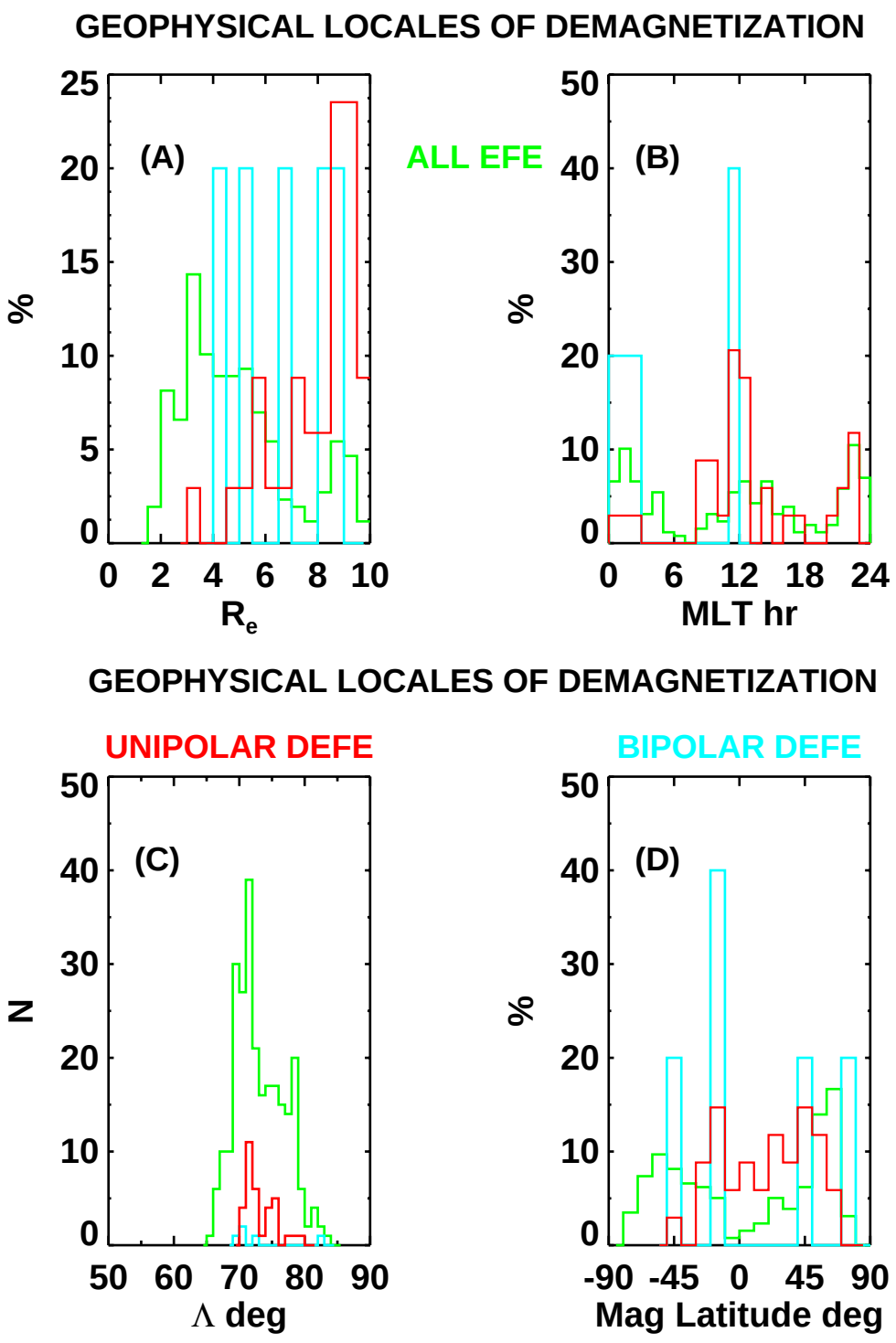
GEOPHYSICAL LOCALES OF DEMAGNETIZATION
(A)
ALL EFE
(B)
%
R_e
MLT hr
GEOPHYSICAL LOCALES OF DEMAGNETIZATION
UNIPOLAR DEFE
BIPOLAR DEFE
(C)
(D)
N
%
Λ deg
Mag Latitude deg

Figure 11

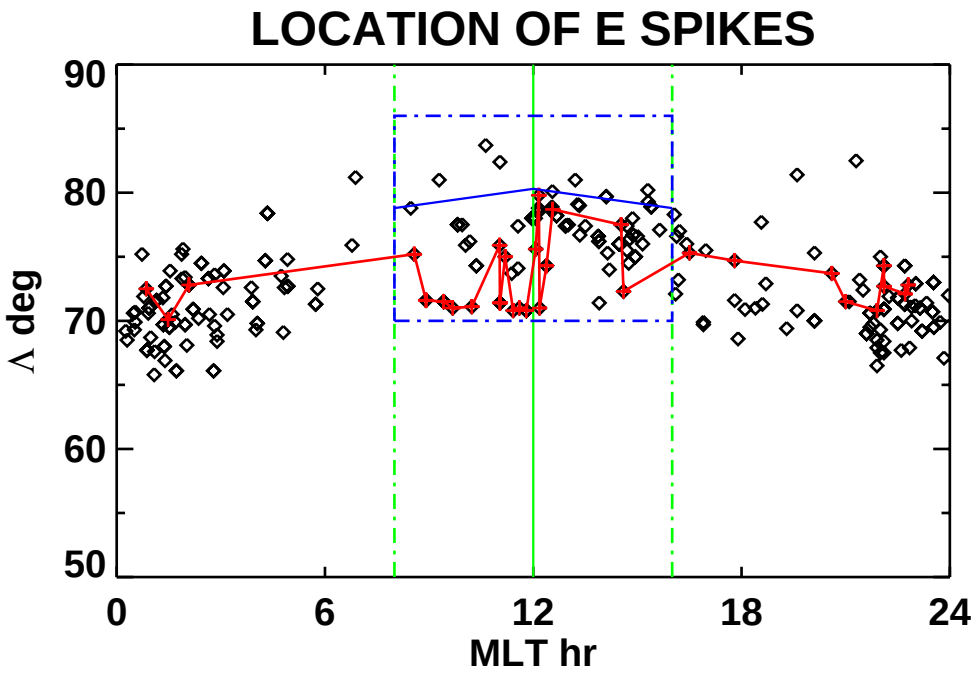

Figure 12